Eur. Phys. J. D **38**, 21–27 (2006)
DOI: 10.1140/epjd/e2005-00312-5

THE EUROPEAN PHYSICAL JOURNAL D

# Energy dependence of the Penning ionization electron spectrum of $Ne^*(^3P_{2,0}) + Kr$

B. Brunetti, P. Candori, S. Falcinelli, B. Lescop, G. Liuti, F. Pirani, and F. Vecchiocattivi[a]

Dipartimento di Chimica e Dipartimento d'Ingegneria Civile ed Ambientale, Università di Perugia, 06100 Perugia, Italy

Received 29 July 2005 / Received in final form 22 August 2005
Published online 16 November 2005 – © EDP Sciences, Società Italiana di Fisica, Springer-Verlag 2005

**Abstract.** A crossed beam experiment is carried out to measure the energy of electrons emitted in Penning ionization processes by $Ne^*(^3P_{2,0})$–Kr collisions. The electron energy spectra have been measured at four different collision energies: 0.050, 0.140, 0.190, 0.460 eV. The analysis of the results allows the separation of spin orbit contributions both in the entrance and in the exit channels providing the related cross-section ratios. Some theoretical considerations have been made to clarify nature and role of interatomic potentials driving the collisions and some general features about the role of atomic fine structure in the Penning ionization processes.

**PACS.** 34.50.Gb Electronic excitation and ionization of molecules; intermediate molecular states (including lifetimes, state mixing, etc.) – 32.70.Jz Line shapes, widths, and shifts

## 1 Introduction

The fine structure of open shell atoms is often of large relevance in many atom-atom or atom-molecule collisional processes, for neutral or charged species as well as in chemical reactivity. It is well established, since long time, that the role of the fine structure in such reactions can be understood in terms of orientation effects of atomic orbitals and therefore can be considered as an important step in understanding the stereodynamics of atomic and molecular processes [1]. In the case of Penning ionization of rare gas atoms by metastable helium or neon, the fine structure effects in the entrance and in exit channels have been studied extensively since long time and many interesting results have been summarized in two review articles [2,3]. While for the Penning ionization by metastable helium atoms the role of fine structure in the exit channels results to be rather clear [2,3], in a recent paper Siska and coworkers [4] point out that some aspects are still to be clarified in the Penning ionization processes involving metastable neon atoms with heavier rare gases. In these systems the fine structure plays a role, not only in the exit channels, but also in the entrance ones.

In 1981, Gregor and Siska [5], on the basis of the analysis of differential scattering and total ionization cross-sections, provided accurate optical potentials for the Ne*–Ar, Kr and Xe systems. These authors also gave an interesting description of the dynamics of the Penning ionization occurring in such systems. Their potentials have been also used successfully for describing some total ionization cross-sections measured in our laboratory [6,7] while the one for Ne*–Ar has been slightly refined by a multiproperty analysis by Baudon et al. [8]. The use of laser quenching selection for the two $J$ states of Ne* [9–12] allowed to obtain separately ionization cross-sections [11–14] and electron spectra [10] for the Penning ionization by $Ne^*(^3P_0)$ or $Ne^*(^3P_2)$. In spite of some theoretical work [15–17], some points remain still unclear: the total ionization cross-section for the $Ne^*(^3P_0)$, $Q_0$, is always larger than that for $Ne^*(^3P_2)$, $Q_2$, and the $Q_0/Q_2$ cross-section ratio has the tendency to increase as the collision energy increases [15–17]. Moreover, it appears from the experiments that the partial cross-section ratio for the two spin orbit components, $^2P_{3/2}$ and $^2P_{1/2}$, of the ionic product, $Q_{3/2}/Q_{1/2}$, is different for the two $J$ states of the metastable neon atom [2,10,14,18], indicating a role also of the Π symmetry, in addition to the Σ one, in the electron exchange mechanism responsible for the ionization, as is well described by theoretical considerations [2,16].

The present paper reports on the electron energy spectra measured for the Ne*–Kr system at four different collision energies. In the experiment, the two fine structure components of metastable neon atoms have been not selected. However, the measured electron spectra have enough energy resolution to allow us to separate the contributions of the spin orbit components in the entrance and in the exit channels.

[a] e-mail: vecchio@dyn.unipg.it

In the paper we also report on some theoretical considerations concerning the interatomic potentials in order to clarify some general features of the fine structure role in the Penning ionization.

## 2 Experimental

The crossed beam apparatus that we have used for the present experiment is a modification of a previous experimental system, already working in our laboratory for mass spectrometric studies of Penning ionization processes and it has been described in detail elsewhere [3,19]. The modification consists in the presence of a hemispherical electron energy analyzer located above the crossed beam region to carry out the energy analysis of electrons emitted by the autoionizing collision complex. Some electron energy spectra measured with this apparatus have been already presented in a very recent paper [19].

Basically, the experimental set-up consists of two crossed beams, one of metastable rare gas atoms and the other one of target ground state species. This latter beam comes from a glass microcapillary array kept at room temperature, while the primary beam was produced by an effusive or supersonic source coupled with different excitation devices, such as microwave discharge or electron impact, as described below. The target beam is monitored by a total ionization detector consisting of an open ionization gauge. It can be assumed that this beam has a Maxwellian velocity distribution, with the most probable velocity, $v_{2w}$, given by the usual relationship $v_{2w} = (2RT/M)^{1/2}$. The two beams cross at right angles in the center of an extracting field which allows the electrons to be extracted and focused into a hemispherical electron energy analyzer and finally detected by a channel electron multiplier.

In these experiments a supersonic source, coupled with an electron bombardment excitation, has been exploited to produce intense and nearly monoenergetic metastable atom beams. To allow for a controlled variation of the collision energy, the source has been used at an adjustable temperature from room up to ∼600 K. With this configuration, Penning ionization electron spectra at four different collision energy values, i.e. 0.050, 0.140, 0.190, 0.460 eV, have been measured. In all cases the velocity distribution of the metastable atoms has been checked by the use of a time-of-flight measurement, obtaining a full width at half maximum of about 10%.

The electrons produced by the Penning ionization have been analyzed at 90° to the beam plane by a hemispherical selector. For the case of 0.050 eV collision energy, the electron energy resolution has been set to ∼25 meV at a transmission energy of 3 eV. However, for the higher collision energies, a resolution of ∼80 meV has been applied in order to increase the electron signal. We have checked that this lower resolution does not affect sensibly the measured cross-section ratios. Spurious effects due to the geomagnetic field have been reduced to ≤20 mG by a $\mu$-metal shielding.

The experimental system has been checked by measuring the product electron energy distribution in the ionization of Ar atoms by metastable He, that is the mostly studied Penning ionization system [2,3]. A supersonic beam of helium has been excited by electron bombardment and therefore metastable He*($2^3$S) and He*($2^1$S) are produced. In the spectrum, reported in Figure 1, the contributions from the two metastable states appear well separated and also the peaks for the two $J$-states of $Ar^+$ ion. The selector features and the energy scale have been tested and calibrated by measuring the photoelectron spectrum of krypton by Ne I radiation and comparing the spectra with those of Kimura et al. [20]. For such a measurement, a microwave discharge beam source has been used, since this device produces a large amount of photons together with the metastable atoms. In order to reduce the Penning ionization contribution in the electron energy spectrum, the background pressure in the intermediate vacuum chamber, located between the metastable source and the beam crossing chamber, has been increased by switching off its diffusion pump. In Figure 2 the electron energy spectrum obtained with the microwave discharge beam source is

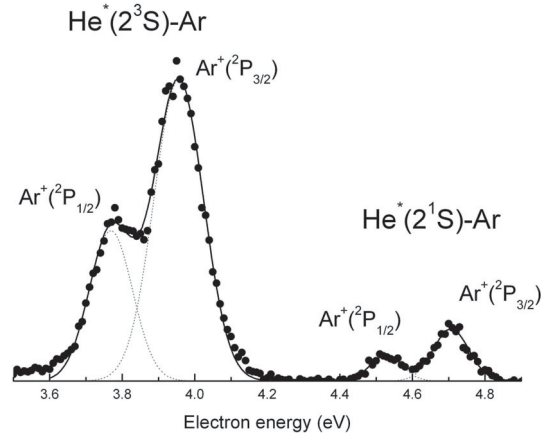


**Fig. 1.** Penning ionization electron spectrum for Ar ionized by metastable helium atoms. For the analysis the spectrum has been decomposed by the use of Gauss functions.

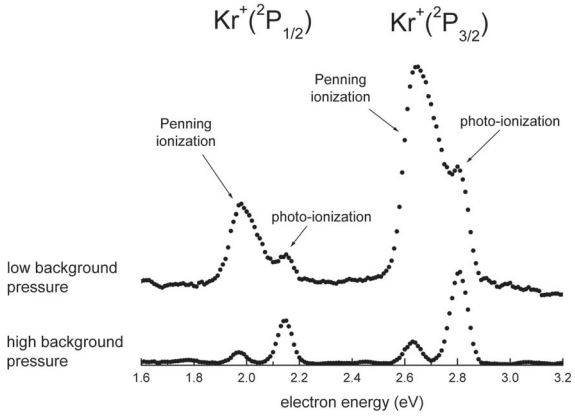


**Fig. 2.** The photoelectron spectrum of Kr by Ne I photons produced by a microwave discharge in neon. The high background pressure in the intermediate vacuum chamber reduces the Penning ionization by a collisional quenching of the metastable neon atoms also produced in the discharge.

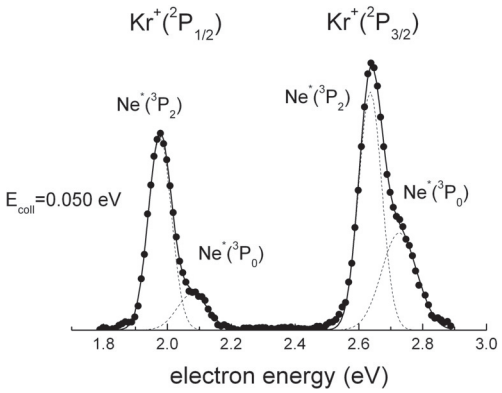


**Fig. 3.** Penning ionization electron spectrum for Kr ionized by metastable neon atoms at a collision energy of 0.050 eV and with a resolution of ∼25 meV. For the analysis the spectrum has been decomposed by the use of Gauss functions.

reported for the two cases with low and high background pressure in the intermediate vacuum chamber. It is well evident the reduction of the Penning ionization peaks due to the increase of the background pressure which causes a collisional quenching of the metastable atoms, but leaving almost unattenuated the Ne I photons.

## 3 Results and data analysis

The spectra for the product electrons obtained for the Ne*–Kr Penning ionization are reported in Figures 3 and 4. While the spectrum at 0.050 eV collision energy, reported in Figure 3, has been measured with ∼25 meV resolution, those in Figure 4 have been recorded for ∼80 meV resolution. In order to obtain the cross-section ratios for the fine structure components in the Ne*–Kr Penning ionization, the spectra have been decomposed in their fine structure contributions. The fit has been accomplished with Gauss functions,

$$y = y_0 + \frac{A}{w\sqrt{\pi/2}} \exp\left[-2\frac{(x-x_c)^2}{w^2}\right] \qquad (1)$$

where $y_0$, $x_c$, $A$, and $w$ are the usual adjustable parameters. This function is symmetric, but it is known that the peaks in this kind of spectra are usually asymmetric, with a tail at higher energies. Therefore, also a fit with the following asymmetric function has been attempted,

$$y = y_0 + A \exp\left[1 - e^{\frac{w}{(x-x_c)}} - \frac{x-x_c}{w}\right]. \qquad (2)$$

The cross-section ratios obtained by fitting the experimental data with the two functions are practically indistinguishable, indicating that the choice of the function to be used for the analysis is not so crucial for our purposes. Moreover, a first attempt of analysis has been performed on the spectrum reported in Figure 1 for He*–Ar, obtaining a ratio $Q_{3/2}/Q_{1/2} = 2.1 \pm 0.2$, in rather good

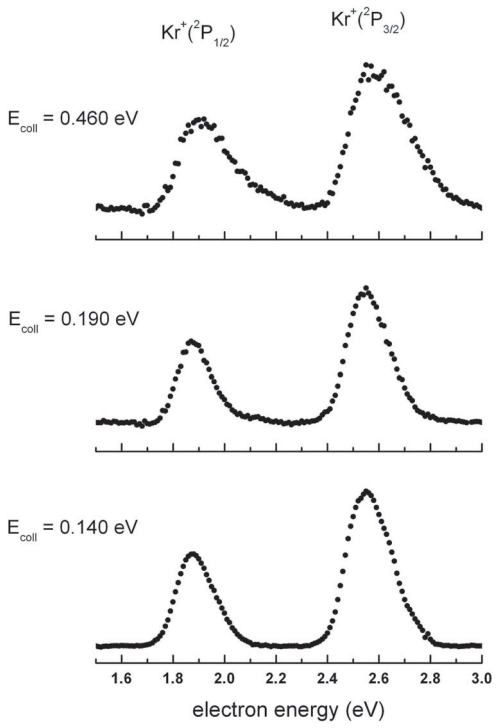


**Fig. 4.** Penning ionization electron spectra for Kr ionized by metastable neon atoms at 0.140, 0.190 and 0.460 eV collision energy and for a resolution of ∼80 meV.

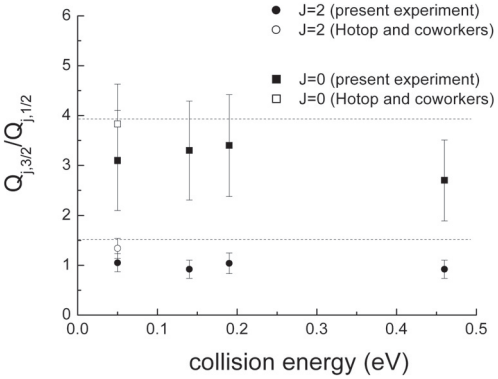


**Fig. 5.** The cross-section ratio for the two fine structure states of the exit channels and for the two $J$ states of the metastable atom in the Ne*–Kr Penning ionization. The present results are compared with those obtained by Hotop and coworkers [10] and with the theoretical ratios [2,16].

agreement with results previously reported by other authors [21–24]. It has to be noted that in the fitting procedure the adjustable parameters in the above functions have been not completely free, since the resulting spin orbit splitting and the peak width are fixed. The results for the Ne*–Kr system are reported in Figure 5, where they are also compared with those reported by Hotop and coworkers [10] by the use of $J$ selected metastable Ne* atoms. The peak shape in the spectrum changes with the collision energy. We did not analyze such a feature, however such a change does not affect the peak ratios that are related to the cross-section ratios [4].

In our Ne*–Kr spectra, the single contributions for the two $J$ states of metastable Ne* can be separated by the spectrum analysis. However, since the $J$ population of our metastable Ne atoms has not been measured, we are unable to deduce the $Q_0/Q_2$ cross-sections ratio.

## 4 Discussion

The He*–Ar system, that we have used here in order to test the present experimental apparatus, has been extensively investigated and rather well understood [2,23–25]. Specifically, the collision dynamics in the entrance channel depends on one potential energy curve of Σ character, while in the exit channels three potential energy curves are possible: one correlating asymptotically with the $Ar^+(^2P_{1/2})$ state and two with the $Ar^+(^2P_{3/2})$ state. For this case, Hoffmann and Morgner [25] gave a very clear explanation by assuming that the ionization occurs through the electron exchange mechanism. Practically, one external $3p$ electron of argon atom goes to fill up the inner-shell $1s$ vacancy of the metastable helium, promoting the passage to the continuum of its $2s$ excited electron. Such a mechanism involves a branching ratio for the two $Ar^+$ fine structure states which reflects the Σ character of the exit channel potential curves.

When the metastable atom is neon, the inner shell vacancy is a $2p$ half filled orbital and therefore the electron exchange mechanism requires a proper alignment of involved orbitals: one is the $2p$ of Ne*, while the other belongs to the partner to be ionized. Some previous investigations [2,16,17] successfully gave account of some characteristics of the fine structure branching ratio of product ion states, but did not explain the different reactivity of the two fine structure metastable sublevels. In this discussion we make some considerations concerning the symmetry character of the interaction potentials, in the Ne*–Kr system, in order to draw some conclusions of general validity for a better understanding of the Penning ionization when Ne* is involved. To do this, we focus our attention on the $(NeKr)^+$ system, since it has been already well established that the external excited electron behaves essentially as a spectator [2–4,15–17,25]. Figure 6 shows a scheme of the Σ and Π symmetry states involved in the coupling by charge transfer in this ionic system.

Within a quantum mechanical framework, some simplifications in the representation of the potential energy are possible by assuming that fine structure effects are neglected in a first step and then reintroduced in a further step. In particular, the interaction energy matrix block-diagonalizes in two $2 \times 2$ sub matrices, one for the Σ and one the Π states, with eigenvalues

$$E_{\pm} = \frac{V_1 + V_2}{2} \pm \sqrt{\left(\frac{\Delta V}{2}\right)^2 + \beta^2}, \qquad (3)$$

where $\Delta V = |V_1 - V_2|$; $V_1$ and $V_2$ are the interactions, without the charge transfer contribution, connecting the molecular states with the asymptotic ones, as schematized

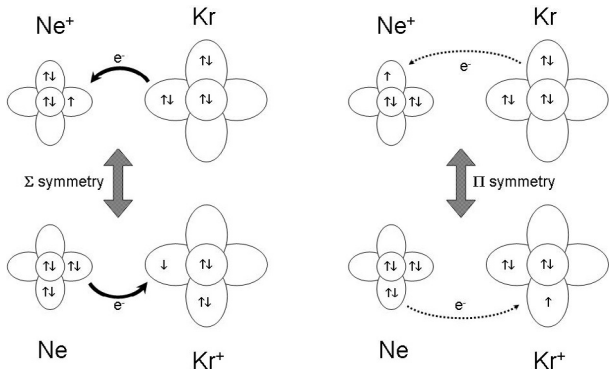


**Fig. 6.** A schematic picture of the Σ and Π symmetry states involved in the coupling by charge transfer in the $(NeKr)^+$ ionic system.

in Figure 6; $\beta$ is the charge transfer coupling matrix element. Obviously, these terms are all depending on the internuclear distance, $R$. From the previous equation one can obtain [26,27]

$$E_+ - E_- = \Delta V + 2V_x \quad \text{or} \quad \beta^2 = V_x(V_x + \Delta V) \qquad (4)$$

where $V_x$ is the "bond stabilization" by charge transfer. When $\Delta V \gg V_x$, one obtains the following perturbative formula:

$$V_x = \frac{\beta^2}{\Delta V}. \qquad (5)$$

Therefore, $V_x$ represents the amount of "stabilization energy", for the state lying below, and of "de-stabilization energy", for the state lying above.

It is well-known that $\beta$ is directly proportional to the overlap integral between the orbitals exchanging the electron [27–29]. Therefore, since one expects that $\beta$ for Π symmetry is about one order of magnitude smaller than for Σ symmetry, $V_x$ becomes of relevance only for Σ symmetry states.

Following the guidelines extensively developed in our laboratory [1,3,6,30–32], when an open shell atom approaches a closed shell atom, it is possible to describe the dependence on $R$ of the potential energy by effective adiabatic potential energy curves, that include interactions for Σ and Π states, $V_\Sigma$ and $V_\Pi$, and spin orbit effects. It is convenient to use for such a description the $V_0$ and $V_2$ Legendre coefficients defined as $V_0 = (V_\Sigma + 2V_\Pi)/3$ and $V_2 = 5(V_\Sigma - V_\Pi)/3$. In this way all anisotropic contributions arising from the stereo-selectivity of charge transfer effects are directly affecting only the $V_2$ term, being $V_0$ the spherical average interaction [26,27]. In the case of $^2P_J$ open shell atoms, with a reversed sequence of fine structure levels, like $Ne^+$ and $Kr^+$, the effective adiabatic potential curves $V_{J\Omega}$, where $\Omega$ is the quantum number

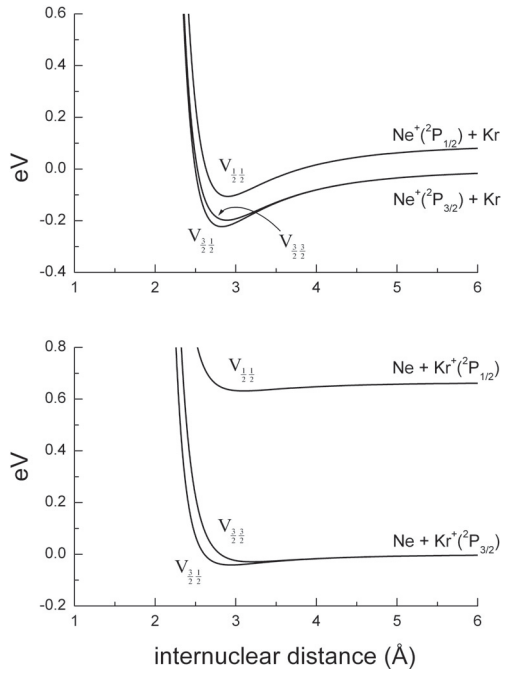


**Fig. 7.** The effective adiabatic potential energy curves $V_{J\Omega}$ for the $(NeKr)^+$ system.

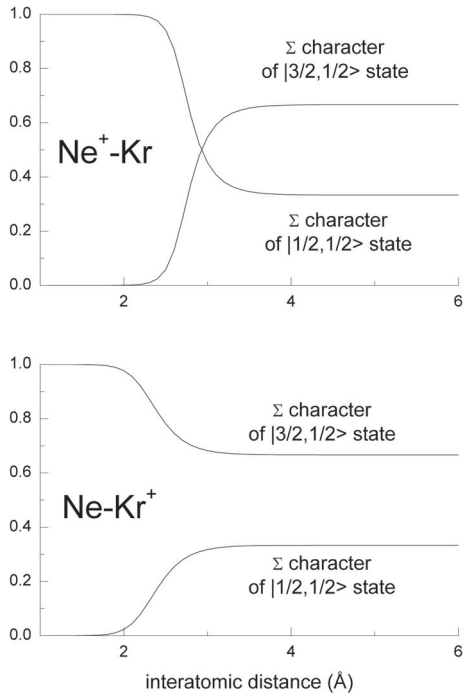


**Fig. 8.** The dependence on the internuclear distance of the Σ character of the $|J,\Omega\rangle$ states. Those of the $|3/2,3/2\rangle$ states are not reported because are zero at all distances.

defining the projection of **J** along $R$, are given by [1,3]

$$V_{|3/2,3/2\rangle} = V_0 - \frac{1}{5}V_2 \tag{6a}$$

$$V_{|3/2,1/2\rangle} = V_0 + \frac{1}{10}V_2 + \frac{1}{2}\Delta - \frac{1}{2}\left(\frac{9}{25}V_2^2 + \Delta^2 - \frac{2}{5}\Delta \cdot V_2\right)^{1/2} \tag{6b}$$

$$V_{|1/2,1/2\rangle} = V_0 + \frac{1}{10}V_2 + \frac{1}{2}\Delta + \frac{1}{2}\left(\frac{9}{25}V_2^2 + \Delta^2 - \frac{2}{5}\Delta \cdot V_2\right)^{1/2} \tag{6c}$$

being $\Delta$ the 3/2–1/2 atomic spin orbit splitting: for $Ne^+$ $\Delta = 0.097$ eV and for $Kr^+$ $\Delta = 0.665$ eV.

We have shown [26,27] that, in the charge transfer perturbative limit, one has $V_2 = 5V_x/2$ and therefore $V_2 < 0$, for the lower Ne–$Kr^+$ state, and $V_2 > 0$, for the upper $Ne^+$–Kr one. Obviously this implies a different correlation between atomic and molecular states at short distances, where $|V_2| > \Delta$: for the molecular states arising from Ne–$Kr^+$, the lowest curve becomes at short distances of Σ character, while for the molecular states arising from $Ne^+$–Kr, the lowest curve becomes of Π character.

The $V_0$ and $V_2$ terms can be evaluated, in a reliable way, following some empirical [33,34] and semiempirical [26,27] formulas, defined in terms of some fundamental physical properties of the separated atoms (charge, ionization potential, polarizability, etc.), reported from our laboratory. The $V_0$ term is given by [35]

$$V_0 = \varepsilon\left[\frac{4}{n(R)-4}\left(\frac{R_m}{R}\right)^{n(R)} - \frac{n(R)}{n(R)-4}\left(\frac{R_m}{R}\right)^4\right]$$

$$n(R) = 9 + 4\left(\frac{R}{R_m}\right)^2 \tag{7}$$

with $\varepsilon = 33.73$ meV and $R_m = 3.08$ Å for Ne–$Kr^+$, and $\varepsilon = 209.4$ meV, $R_m = 2.86$ Å for Ne–$Kr^+$. $V_2$ term is given by $V_2 = \pm 1.6741 \times 10^7 \exp(-4.32R)$ meV, with $R$ given in Å and where the positive sign refers to the upper $Ne^+$–Kr curves, while the negative sign to the lower Ne–$Kr^+$ curves. The relevant curves for the $(NeKr)^+$ ion derived by using equations (6) and (7) are plotted in Figure 7. The dependence of the Σ character of the $|J,\Omega\rangle$ states on the internuclear distance can be studied by using the procedure reported in a previous paper [36]. For the $(NeKr)^+$ ion such a dependence is shown in Figure 8. The different behavior of $Ne^+$–Kr with respect to Ne–$Kr^+$ arises from the opposite sign in $V_2$ and from the different values of $\Delta$. The Σ character of the $|3/2,3/2\rangle$ states is not reported because is zero at all distances.

In the $Ne^*$–Kr interaction, one has a spherically symmetric $3s$ orbital electron wrapping the ionic core and therefore the $V_2$ term is the same of $Ne^+$–Kr discussed above. This leads to a correlation diagram applicable to all the $Ne^*$-heavier rare gas systems and reported in Figure 9.

Assuming the Gregor and Siska potential [5] as the spherical component of the neutral entrance channel interaction and using the $V_2$ term discussed above, we can

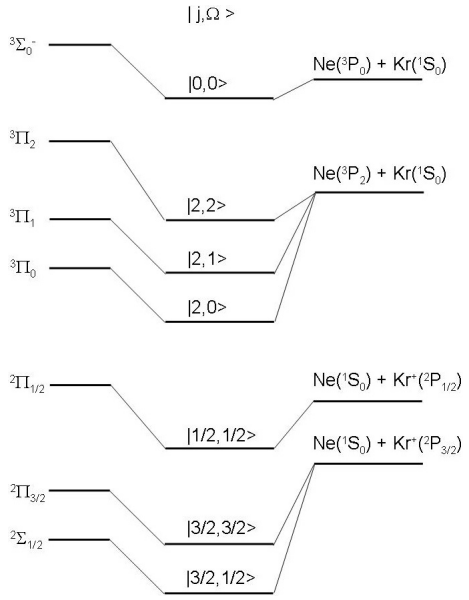


**Fig. 9.** A schematic diagram showing the correlation between molecular and atomic states involved in Ne*–Kr Penning ionization.

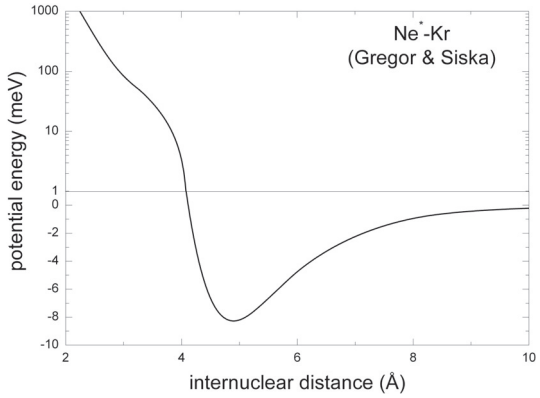


**Fig. 10.** The spherical potential of Ne*–Kr system as obtained by Gregor and Siska [5].

easily obtain the effective $V_{J\Omega}$ adiabatic curves for the Ne*–Kr. The Gregor and Siska potential is plotted in Figure 10, while in Figure 11 the repulsive branch of such a potential is compared with the various $V_{J\Omega}$. The curves appear splitted because of the core anisotropy by a small amount and only at short range, indicating that the core anisotropy does not play an important role due to the shielding effect of excited electron of Ne* in the 3*s* spherically symmetric orbital, as already suggested by Gregor and Siska [5]. Within an optical potential model description of the Penning ionization [2,3], this consideration applies only to the real part of the potential, while we should expect that the imaginary part is strongly affected by the anisotropy in the $\beta$ term, when the electron exchange mechanism is operative. Therefore, the imaginary part is expected to be much more stereoselective than the real part, and the Σ and Π character of the interaction and

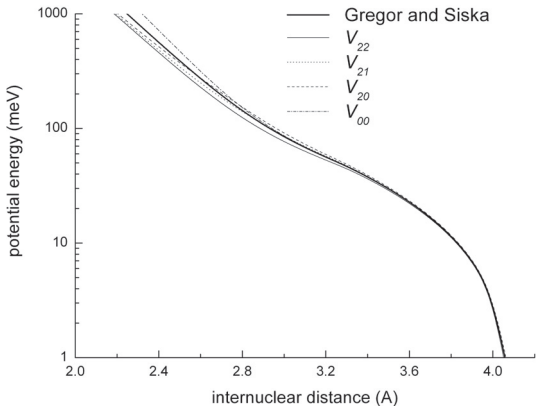


**Fig. 11.** The repulsive branch of the Gregor and Siska potential (see Fig. 10) for the Ne*–Kr interaction, compared with the various $V_{J\Omega}$.

their dependence on $R$ is strongly affecting the ionization probability and its collision energy dependence [4].

A very important feature comes from all the above considerations: the $|2,2\rangle$ state has a pure Π character at all distances, the $|2,1\rangle$ and $|2,0\rangle$ states have a Σ character decreasing when $R$increases, while the $|0,0\rangle$ state increases the Σ character when the distance decreases. This partially modifies the sequence of short distance states that has been published previously [2,4–6,15–17] and qualitatively justifies the increase with the collision energy of the total ionization cross-section ratio for the two states of the metastable neon atom, $Q_0/Q_2$, interacting with a species with an ionization potential lower than that of the ground state neon atom. This experimental finding has been found by Bejierinck and coworkers [11–13], and recently also by Siska and coworkers [4] for Ne*–Ar and by us for Ne*–$N_2O$ system [19].

About the $Q_{3/2}/Q_{1/2}$ exit channel branching ratio, it has been extensively discussed by Morgner [16], and later on also by Siska and coworkers [2,4], that such a branching ratio does not depend on the features of the entrance channels, but only on the characteristics of the exit channels. If one assumes that the Σ and Π characters of the exit ionic system does not change too much in the distance range probed by the experimental collision energy, the branching ratio is constant with values $Q_{3/2}/Q_{1/2} = 3.94$ for the Ne*($^3$P$_0$) and $Q_{3/2}/Q_{1/2} = 1.51$ for the Ne*($^3$P$_2$) [2,4,16]. Within the experimental uncertainty, our results appear in a satisfactory agreement with such expected values, at least at low collision energy, where they also agree with the experimental results by Hotop and coworkers [10]. It is interesting that for the Ne*–Ar system also Siska and coworkers [4] observed such a nice agreement in the low energy collision limit, while at larger energies the agreement is less satisfactory. The small discrepancies, observed when the energy increases, could be due to the combination of several factors [4] like the change of the Σ and Π characters in the probed internuclear distance and the fact that the theory assumes that the ejected electron comes from the 3*s* orbital. However, the analysis by Gregor and Siska [5] suggests that the interatomic electric field can

favor the passage of such electron in a *spd* hybrid atomic orbital, with possible additional phenomena.

Financial contributions from the MIUR (Ministero dell'Istruzione, dell'Università e della Ricerca) is gratefully acknowledged.

## References


1. V. Aquilanti, G. Liuti, F. Pirani, F. Vecchiocattivi, J. Chem. Soc., Faraday Trans. **85**, 955 (1989)
2. P.E. Siska, Rev. Mod. Phys. **65**, 337 (1993)
3. B. Brunetti, F. Vecchiocattivi, *Current Topic on Ion Chemistry and Physics*, edited by C.Y. Ng, T. Baer, I. Powis (John Wiley & Sons Ltd, New York, 1993), p. 359
4. B.A. Jacobs, W.A. Rice, P.E. Siska, J. Chem. Phys. **118**, 3124 (2003)
5. R.W. Gregor, P.E. Siska, J. Chem. Phys. **74**, 1078 (1981)
6. A. Aguilar, B. Brunetti, S. Rosi, F. Vecchiocattivi, G.G. Volpi, J. Chem. Phys. **82**, 773 (1985)
7. B. Brunetti, F. Vecchiocattivi, G.G. Volpi, J. Chem. Phys. **84**, 536 (1986)
8. J. Baudon, P. Feron, C. Miniatura, F. Perales, J. Reinhardt, J. Robert, H. Haberland, B. Brunetti, F. Vecchiocattivi, J. Chem. Phys. **95**, 1081 (1991)
9. F.B. Dunning, T.B. Cook, W.P. West, R.F. Stebbings, Rev. Sci. Instrum. **46**, 697 (1975)
10. H. Hotop, J. Lorenzen, A. Zastrow, J. Electr. Spectr. Rel. Phenom. **23**, 347 (1981)
11. M.J. Verhein, H.C.W. Beijerinck, Chem. Phys. **102**, 255 (1986)
12. F.T.N. van den Berg, J.H.M. Schonenberg, H.C.W. Beijerinck, Chem. Phys. **115**, 359 (1987)
13. J.P.J. Driessen, H.J.L. Megens, M.J. Zonneveld, H.A.J. Senhorst, H.C.W. Beijerinck, B.J. Verhaar, Chem. Phys. **147**, 447 (1990)
14. C. Weiser, P.E. Siska, J. Chem. Phys. **85**, 4746 (1986)
15. H. Morgner, Comm. At. Mol. Phys. **11**, 271 (1982)
16. H. Morgner, J. Phys. B **18**, 251 (1985)
17. J.P.J. Driessen, S.S. Op de Beek, L.M.T. Somers, H.C.W. Beijerinck, B.J. Verhaar, Phys. Rev. A **44**, 167 (1991)
18. T. Bregel, W. Bussert, J. Ganz, H. Hotop, M.-W. Ruf, in *Electronic and Atomic Collisions, ICPEAC XIV*, edited by D.C. Lorents, W.E. Meyerhof, J.R. Peterson (North-Holland, Amsterdam, 1986), p. 577
19. B. Biondini, B. Brunetti, P. Candori, F. De Angelis, S. Falcinelli, M. Teixidor, F. Pirani, F. Tarantelli, F. Vecchiocattivi, J. Chem. Phys. **122**, 164307 (2005)
20. K. Kimura, S. Katsumata, Y. Achiba, T. Yamazaki, S. Iwata, *Handbook of He I Photoelectron Spectra of Fundamental Organic Molecules* (Japan Scientific Press, Tokyo, 1981)
21. H. Hotop, in *Electronic and Atomic Collisions, ICPEAC XI*, edited by N. Oda, K. Takayanagi (North-Holland, Amsterdam, 1980), p. 271
22. A. Le Nadan, G. Sinou, F. Tuffin, Chem. Phys. Lett. **156**, 24 (1989)
23. E.J. Longley, D.C. Dunlavy, M.F. Falcetta, H.M. Bevsek, P.E. Siska, J. Phys. Chem. **97**, 2097 (1993)
24. K. Ohno, H. Yamakado, T. Ogawa, T. Yamata, J. Chem. Phys. **105**, 7536 (1996)
25. V. Hoffmann, H. Morgner, J. Phys. B **12**, 2857 (1979)
26. V. Aquilanti, D. Cappelletti, F. Pirani, Chem. Phys. Lett. **271**, 216 (1997)
27. F. Pirani, A. Giulivi, D. Cappelletti, V. Aquilanti, Mol. Phys. **98**, 1749 (2000)
28. J.L. Magee, J. Chem. Phys. **8**, 687 (1940)
29. R. Grice, D.R. Herschbach, Mol. Phys. **27**, 159 (1974)
30. V. Aquilanti, G. Grossi, J. Chem. Phys. **73**, 1165 (1980)
31. V. Aquilanti, P. Casavecchia, G. Grossi, A. Laganà, J. Chem. Phys. **73**, 1173 (1980)
32. V. Aquilanti, R. Candori, F. Pirani, J. Chem. Phys. **89**, 6157 (1988)
33. R. Cambi, D. Cappelletti, G. Liuti, F. Pirani, J. Chem. Phys. **95**, 1852 (1991)
34. D. Cappelletti, G. Liuti, F. Pirani, Chem. Phys. Lett. **183**, 297 (1991)
35. F. Pirani, M. Albertì, A. Castro, M. Moix Teixidor, D. Cappelletti, Chem. Phys. Lett. **394**, 37 (2004)
36. P. Tosi, O. Dmitrijev, Y. Soldo, D. Bassi, D. Cappelletti, F. Pirani, V. Aquilanti, J. Chem. Phys. **99**, 985 (1993)